Inorganic Chemistry

Article

pubs.acs.org/IC

Effect of Nitrogen-Containing Impurities on the Activity of Perovskitic Catalysts for the Catalytic Combustion of Methane

Olga Buchneva,[†] Alessandro Gallo,[‡,§] and Ilenia Rossetti*[,†,⊥]

[†]Dipartimento Chimica Fisica ed Elettrochimica, Università degli Studi di Milano, and INSTM Unit Milano-Università, via C. Golgi 19, I-20133 Milano, Italy

[‡]CNR—Istituto di Scienze e Tecnologie Molecolari, via Fantoli 16/15, Milano I-20128, Italy

[⊥]CNR—Istituto di Scienze e Tecnologie Molecolari, via C. Golgi 19, I-20133 Milano, Italy

ABSTRACT: $LaMnO_3$, either pure or doped with 10 mol % Sr, has been prepared by flame pyrolysis in nanostructured form. Such catalysts have been tested for the catalytic flameless combustion of methane, achieving very high catalytic activity. The resistance toward poisoning by some model N-containing impurities has been checked in order to assess the possibility of operating the flameless catalytic combustion with biogas, possibly contaminated by S- or N-based compounds. This would be a significant improvement from the environmental point of view because the application of catalytic combustion to gas turbines would couple improved energy conversion efficiency and negligible noxious emissions, while the use of biogas would open the way to energy production from a renewable source by means of very efficient technologies. A different behavior has been observed for the two catalysts; namely, the undoped sample was more or less heavily poisoned, whereas the Sr-doped sample showed slightly increasing activity upon dosage of N-containing compounds. A possible reaction mechanism has been suggested, based on the initial oxidation of the organic backbone, with the formation of NO. The latter may adsorb more or less strongly depending on the availability of surface oxygen vacancies (i.e., depending on doping). Decomposition of NO may leave additional activated oxygen species on the surface, available for low-temperature methane oxidation and so improving the catalytic performance.

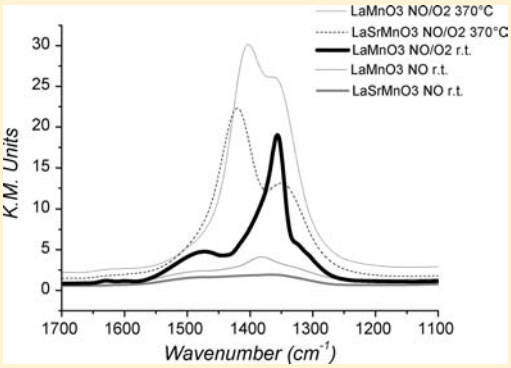

1. INTRODUCTION

Natural gas (NG) is composed of 85−95 mol % CH_4, plus CO_2, N_2, and small amounts of heavier hydrocarbons. NG is usually odorized at the ppm level with S-based compounds to allow its detection by smell. By contrast, biogas (BG) typically refers to a gas produced by anaerobic digestion or fermentation of organic matter, including manure, sewage sludge, municipal solid wastes, or any other biodegradable waste or feedstock. BG is composed primarily of CH_4 and CO_2, and if properly cleaned up, it has the same characteristics of NG. However, the presence of different impurities is envisaged in BG depending on the widely variable feedstocks employed for its production.

The low-temperature flameless combustion of methane attracts interest because of lower emissions of nitrogen oxides (NO_x), carbon monoxide, and unburned hydrocarbons with respect to homogeneous combustion. Perovskite-like catalysts proved satisfactory for the deep oxidation of hydrocarbons.[1] The catalytic activity was found to be dependent not only on the composition of the catalysts[2−4] but also on the preparation procedure.[5,6]

One of the key topics for the practical application of catalytic combustion technology is the sensitivity of the catalyst to different poisoning agents. The most frightening poisons are S-containing molecules possibly present in NG or BG. Li et al.[7] studied poisoning by SO_2 of $La_{1-x}A_xMnO_3$, where A = Sr, Ba, Ca, and Pb and x = 0.3 or 0.5, showing that these catalysts were severely and irreversibly poisoned by 50 ppm SO_2 at 240−300 °C. Tejuca et al.[8] confirmed the dramatic decrease of the methane oxidation rate in the presence of small amounts of SO_2. Sulfur species can indeed adsorb on the active sites of the catalyst surface.

Different strategies of protection were suggested in the literature.[7,9] Many of them are based on the addition of a promoter or dopant, either into the framework or in the extraframework position, that can react with sulfur more promptly, leading to a sort of "shield effect". Our previous research[10,11] showed that catalysts prepared by flame pyrolysis (FP) led not only to an improvement of the catalytic activity but also to a different sensitivity to poisoning by an S-containing model molecule.

Other impurities that may be present in BG streams are N-containing compounds.[12,13] The BG produced from anaerobic digestion of biowaste (i.e., animal manure) could contain ammonia, up to 2000 ppm. Also, in many gaseous emissions (i.e., from C-based and petrochemical processes, treatment of solid wastes and wastewater, etc.), methane is accompanied by other inorganic and organic N-containing compounds. In the

Received: July 20, 2012
Published: October 5, 2012

   dx.doi.org/10.1021/ic3015892 | *Inorg. Chem.* 2012, 51, 11680−11687

Table 1. Activity Data of Fresh and Poisoned Catalysts, i.e., after Injection of an Amount Corresponding to 80 and 240 h On-Stream with 1 ppm of N-Containing Model Compounds[a]

		fresh catalyst		poisoned catalyst		
sample	poisoning agent	T_{50}	$conv_{450}$, %	80 h, $conv_{450}$, %	240 h, $conv_{450}$, %	Δ, % (240 h)
$La_{0.9}Sr_{0.1}MnO_3$	pyrrolidine	433	65	67.5	69	+4
$La_{0.9}Sr_{0.1}MnO_3$	piperidine			62.8	62.8	−2.2
$La_{0.9}Sr_{0.1}MnO_3$	pyrrole			70		+5
$La_{0.9}Sr_{0.1}MnO_3$	pyridine			66	66	+1
$La_{0.9}Sr_{0.1}MnO_3$	ammonia			64.3	60.6	−4.4
$LaMnO_3$	pyrrolidine	438	58	53	43.5	−14.5
$LaMnO_3$	piperidine			48	48	−10
$LaMnO_3$	pyrrole			54		−4
$LaMnO_3$	pyridine			56	52	−6
$LaMnO_3$	ammonia			58	58	0

[a] T_{50} = temperature of 50% CH_4 conversion; $conv_{450}$ = CH_4 percent conversion at 450 °C. Activity data for poisoned samples are given as residual CH_4 percent conversion at 450 °C. Δ = activity variation due to poisoning (conversion of fresh sample − residual conversion after the last poisoning cycle) expressed in points percent.

case of coke oven emission, for example, benzene, toluene, CO, CO_2, NO, H_2, H_2O, NH_3, and other compounds are present,[14−16] which may possibly alter the catalytic activity.

Therefore, in the present work, we investigated the influence of different types of N-containing model compounds on the low-temperature catalytic combustion of methane. $LaMnO_3$ and $La_{0.9}Sr_{0.1}MnO_3$ were chosen as catalysts because, in our previous research, both showed satisfactory results not only from the point of view of their catalytic activity but also for their resistance to poisoning.

N-containing molecules of different nature (inorganic, aromatic, aliphatic, and heterocyclic compounds) have been tested, and a possible mechanism for their interaction with the catalytic active sites has been proposed.

2. EXPERIMENTAL SECTION

2.1. Catalyst Preparation. Every sample was prepared by FP. All of the precursor solutions were prepared by dissolving in propionic acid (Aldrich, purity 97%) and the salts of the selected metals, $La(CH_3COO)_3·2H_2O$ (Aldrich, purity 99.9%), $Mn(CH_3COO)_2·4H_2O$ (Aldrich, purity 99%), and $Sr(CH_3COO)_2$ (Aldrich, purity 99%), in the desired ratio and metal concentration. The FP apparatus has been described in detail elsewhere.[17] Briefly, it consists of a capillary tube (inner diameter 0.6 mm) ending in the center of a vertical nozzle and connected with a syringe pump (Harvard, model 975), feeding the solution of the mixed oxide precursors. The nozzle is cofed with oxygen (SIAD, purity >99.95%, flow rate 5 L min^{-1} STP), acting both as an oxidant and as a dispersing agent, able to form microdroplets of solution. The gas flow rate was regulated by MKS (model 1259C) mass flowmeters, controlled by a MKS (model 247C) control unit. The synthesized nanoparticles were collected by means of a 10 kV electrostatic precipitator.

2.2. Catalyst Characterization. The crystal structure of the prepared samples was determined by powder X-ray diffraction (XRD) on a Philips PW3020 instrument. The patterns obtained were compared with literature data for phase recognition.[18] The surface area of the synthesized powders was measured by N_2 adsorption/desorption at −196 °C on a Micromeritics ASAP2010 apparatus, after outgassing at 300 °C overnight.

NO-pulsed chemisorption experiments were carried out at room temperature (rt) after pretreatment of the sample under O_2 flow (20 cm^3 min^{-1} STP; 20 vol % in He) at 500 °C for 1 h in a homemade apparatus.[19] Typically, 70 mg of the samples was loaded inside a U-shaped Pyrex reactor connected upstream to a gas feeding device, and pulses of 50 μL of NO/Ar mixture (50 vol %) were admitted in the reactor using He (20 mL min^{-1} STP) as the carrier gas until the signal intensity of the outflowing pulses was constant. A quadrupole mass spectrometer was used as the detector (HPR-20 QIC gas analysis mass spectrometer system, Hiden Analytical Ltd.).

NO temperature-programmed desorption (NO-TPD) was performed after chemisorption in the same apparatus. The sample was heated by 10 °C min^{-1} under a He flow (20 cm^3 min^{-1} STP) up to 500 °C, and the evolution of NO, NO_2, N_2O, N_2, and O_2 was monitored.

Diffuse-reflectance infrared Fourier transform (DRIFT) spectra were recorded using a homemade DRIFTS reaction chamber inserted in a FTS-60A spectrometer, equipped with mercury−cadmium telluride detector. The sample, diluted 1:7 (w/w) with KBr, was pretreated under O_2 (20 vol % in He) at 500 °C for 1 h before analysis. The spectra were collected using a resolution of 4 cm^{-1} and accumulating 100 scans. Measurements recorded with KBr under a He flow were used for a background spectrum. The samples were saturated with 1 vol % NO in He (20 cm^3 min^{-1} STP) at rt or 0.8 vol % NO and 20 vol % O_2 (20 cm^3 min^{-1} STP) at 370 °C. A simulation of the reaction was also performed in the same reactor, admitting pure CH_4 at 370 °C over the sample presaturated in NO or in a NO/O_2 atmosphere.

Thermogravimetric analysis (TGA) experiments were performed in a Perkin-Elmer TGA7 apparatus under an air flow with a heating rate of 2 °C min^{-1} from rt to 1000 °C. Alternatively, the sample was calcined in situ at 900 °C under flowing air for 1 h, and then the analysis was preformed under N_2 using the same thermal ramp specified above, without significant differences.

Temperature-programmed reduction (TPR) experiments were carried out using a Micromeritics PulseChemisorb 2700 instrument. Around 30 mg of each sample was loaded in a U-shaped Pyrex reactor and calcined at 900 °C under a O_2 flow. TPR analysis followed under 15 cm^3 min^{-1} STP H_2/8 vol % Ar flow, with a 8 °C min^{-1} heating rate.

2.3. Catalytic Activity Testing. Catalytic activity tests were carried out in a continuous quartz tubular reactor with ca. 0.15 g of catalyst, pelletized, ground, and sieved to 0.15−0.25 mm particle size. Prior to each run, the catalyst was activated in flowing air (20 cm^3 min^{-1} STP) with increasing temperature by 10 °C min^{-1} up to 600 °C and then kept for 1 h. The activity tests were carried out by feeding a mixture composed of 0.34 vol % CH_4, 33.3 vol % air, and He balance, while increasing the temperature by 10 °C min^{-1} from 200 up to 600 °C. Such a gas composition has been selected to obtain sufficiently high sensitivity to concentration changes of methane but a negligible hot spot across the catalyst bed. The gas flow rate was regulated by means of mass flowmeters (Brooks Instruments, model 5850) governed by a control unit (Brooks, model 0154). The total gas flow rate was 30 cm^3 min^{-1} STP. The outcoming gas was analyzed in line by means of a quadrupolar mass spectrometer (MKS, PPT residual gas analyzer), selecting proper mass fragments.

Catalyst poisoning was done in the same apparatus at 450 °C by injecting appropriate amounts of poisoning agent per 1 g of catalyst.

dx.doi.org/10.1021/ic3015892 | Inorg. Chem. 2012, 51, 11680−11687

The selected doses of nitrogen compounds correspond to 80 and 240 h of continuous flow with 1 ppm. Pyrrolidine, pyrrole, piperidine, pyridine, and a 4 vol % ammonia solution in water were chosen as a poisoning agent. For the latter option, a blank test injecting the corresponding amount of water was also carried out, with a negligible effect on the activity. Because of the low volatility of pyrrole, only the amount corresponding to 80 h onstream at the 1 ppm level was used. The catalytic activity was monitored *operando* during poisoning, by continuously analyzing the relevant mass fragments (CH_4, NO, N_2, NO_2, CO, CO_2, and H_2O) and plotting them as partial pressure versus time. A standard activity test was then repeated after each poisoning cycle.

3. RESULTS AND DISCUSSION

3.1. Catalytic Activity and Effect of N-Containing Impurities. Both catalysts showed a high activity for the oxidation of methane. Under the reaction conditions adopted, full methane conversion was achieved below 600 °C. No conversion in this temperature range was observed in the absence of the catalyst. Water and carbon dioxide were the only detected products. For the practical quantification of activity results, the temperature corresponding to half methane conversion (T_{50}) is reported here. The results of activity testing on the fresh samples are reported in Table 1.

Doping with Sr slightly improved the catalytic activity because T_{50} decreased from 438 °C for $LaMnO_3$ to 433 °C for $La_{0.9}Sr_{0.1}MnO_3$, as was already reported elsewhere.[6]

Sr doping should lead to an increase of the oxygen vacancy concentration, as well as to an increase of the Mn ion formal oxidation state. In general, cation substitution in the perovskite structure is an important instrument to tune the catalytic activity considering both the suprafacial and intrafacial reaction mechanisms.[20] For instance, the suprafacial mechanism can be affected by changing the electronic configuration of the d element, also based on a possible synergistic effect because of the combination of different elements at the B position. By contrast, the intrafacial mechanism can be improved by different types and concentrations of lattice defects, in turn affecting the oxygen mobility through the framework. However, the influence of the doping cations on the catalytic activity depends on the catalyst formulation and, at least to our knowledge, there is no consolidated theory really allowing one to predict the influence of dopants.

Poisoning of the catalysts led to different results depending on the composition of the gas stream and the poisoning agent, as is shown in Table 1. To compare the effect of the N-containing compound, conversion of methane at 450 °C was chosen. This temperature has been chosen because both samples exhibit the highest reaction rate around this value and the conversion curve is very steep and so the effect of the impurity can be magnified.

In contrast with that reported in the literature,[21−23] nitrogen compounds led to evident poisoning of the native $LaMnO_3$ sample, with a less marked effect of the aromatic heterocyclic species. Reasonably, being more stable, their decomposition was less efficient with respect to the nonaromatic ones, thus making more difficult the following poisoning mechanism. By contrast, ammonia did not alter the catalytic activity of this sample. Therefore, a competitive mechanism was observed between methane combustion and some N-containing poisons in the case of $LaMnO_3$.

The catalysts doped with Sr showed better resistance to poisoning. Its activity remained approximately constant or even increased after injection of the highest amount of N-containing impurity. The conversion of methane at 450 °C increased in almost all cases, except with ammonia and piperidine. The poisoning of the undoped catalyst led to an increase of the ignition temperature by 20−30 °C. On the contrary, the Sr-substituted catalyst did not show changes in the ignition temperature.

In order to deal with this different behavior, we tried to hypothesize a possible mechanism of interaction between the catalyst and the N-containing molecule. In general, organic nitrogen compounds could decompose with the formation of a wide number of intermediates, such as methylamine, cyanic acid, nitrogen oxides, and nitrogen. Koger and Bockhorn[24] showed that at 917 °C ammonia immediately decomposed in the presence of methane. At this temperature, the formation of HCN was also observed. Under these conditions, HCN is an intermediate species, being converted into N_2 and NO_x under an oxidizing atmosphere. The possible desorption of N_2O is unlikely because it is unstable and oxidizes promptly to NO. The decomposition of more complex organic molecules is also believed to occur through the formation of HCN.[25,26] Under fuel-lean conditions, HCN is converted into NO and N_2 immediately above 907 °C.[24] Because of the gas-phase reaction between oxygen and NO, NO_2 could also form.

Our experimental results evidenced the evolution of NO at least partially desorbing from each sample (Figure 1a), with a more pronounced retention for $La_{0.9}Sr_{0.1}MnO_3$ (smaller area of the first peak). Furthermore, the MS signal of NO_2 exhibited a much lower intensity, comparable to the background noise, and some desorption was observed for the Sr-doped sample during each pulse at 450 °C, while NO_2 desorption was undetectable for the undoped manganite (Figure 1b). No peaks of N_2,

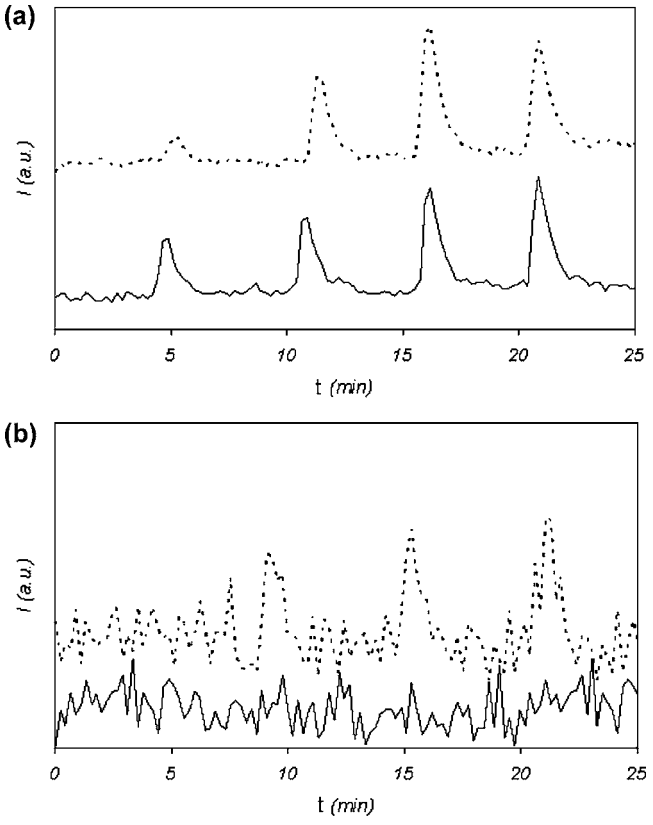

Figure 1. Emission of (a) NO and (b) NO_2 during poisoning with piperidine for $LaMnO_3$ (solid line) and $La_{0.9}Sr_{0.1}MnO_3$ (dotted line).

dx.doi.org/10.1021/ic3015892 | Inorg. Chem. 2012, 51, 11680−11687

possibly generated by NO decomposition, were evident because of the too high background level for N_2 species. Apparently, no HCN was released as such from the sample.

It has been proposed in some cases that NO adsorbs with the N atom nearest the surface, although some authors have also suggested the opposite allocation, i.e., with the O atom coordinated to anion vacancies at the surface. During NO adsorption on metal oxides, charge transfer may also occur via an electron from the oxide to the antibonding orbital of the NO molecule, thus reducing the NO bond order from 2.5 to 2.0 and making the molecule less stable than in its native state. However, some experiments[27] have shown electron transfer in the opposite direction, to form NO^+ species, which promotes to a bond order of 3.0. In such a case, NO should dissociate harder than the neutral NO molecule.

Rare-earth oxides[28] are active for NO decomposition. The decomposition of NO into N_2 and O_2 is thermodynamically favorable below 1027 °C, and several perovskite-type oxides exhibit good performance for the decomposition of NO already above 450 °C. The reaction of NO molecules on the active sites is assumed to occur stepwise. We may then postulate the following mechanism. NO is adsorbed by locating its oxygen into a surface oxygen vacancy, and an electron is transferred to the NO molecule from a B-site cation neighboring the vacancy. NO^- species form with the concomitant oxidation of the B-site cation ($Mn^{3+} \rightarrow Mn^{4+}$). Once a second NO molecule adsorbs, a free N_2 molecule is released into the gas phase from the interaction of two neighboring NO^- species. The release of oxygen is regulated by its adsorption−desorption equilibrium, and the formation of two oxygen vacancies with the release of O_2 involves a four-electron process, very unlikely especially at low temperature. Therefore, spontaneous NO decomposition is very slow, and to efficiently convert NO to N_2, a reducing agent should be conveniently added.[29] A promotional effect of CH_4 on NO conversion to N_2 might thus be expected on the basis that CH_4 can facilitate the removal at relatively low temperature of surface oxygen left behind by the decomposition of nitrogen oxide species, renewing oxygen vacancies available for the activation of O_2 or for the adsorption of additional NO.

According to this hypothesis, NO adsorption and its possible subsequent decomposition should increase with the concentration of oxygen vacancies, i.e., in principle, for the Sr-doped sample. For the latter catalyst, the formation of activated oxygen upon NO decomposition may improve the catalytic activity through the suprafacial mechanism, as is indeed observed in the present case. Indeed, activated surface oxygen species may play a role in the low-temperature activity typical of the suprafacial mechanism. This is also in agreement with the results of Zhang et al.,[27] who showed a positive effect of Sr doping for NO reduction.

The possible effect of O_2 present in the reaction environment should also be considered. An excess of oxygen promotes NO reduction by CH_4 over all of the catalysts. In the presence of oxygen, two competitive reactions exist for methane, namely

$$CH_4 + 2NO + O_2 \rightarrow N_2 + CO_2 + 2H_2O$$

$$CH_4 + 2O_2 \rightarrow CO_2 + 2H_2O$$

The role of oxygen in NO reduction over rare-earth oxides is not univocal because the formation of NO_2 is also possible, as suggested for zeolite catalysts. It has been further reported that $CH_3^\bullet$ radicals are generated at 450 °C. Therefore, the involvement of methyl (or methylene) surface species to reduce NO under reaction conditions seems very likely.[30]

We may therefore postulate that the addition of N-containing compounds to CH_4 ends in the formation of NO, more or less easily depending on the backbone of the molecule and its oxidability. NO may decompose to N_2 and activated oxygen species. This is favored by the presence of oxygen vacancies on the catalyst surface (i.e., with the Sr-doped sample) able to coordinate and further process NO. Increasing CH_4 conversion, as evidenced by the present data for the $La_{0.9}Sr_{0.1}MnO_3$ sample, may be explained by the surplus availability of activated surface oxygen.

To check these hypotheses, the evolution of NO and NO_2 during the activity test carried out after poisoning has been recorded, and it is shown in Figure 2. NO did not desorb as

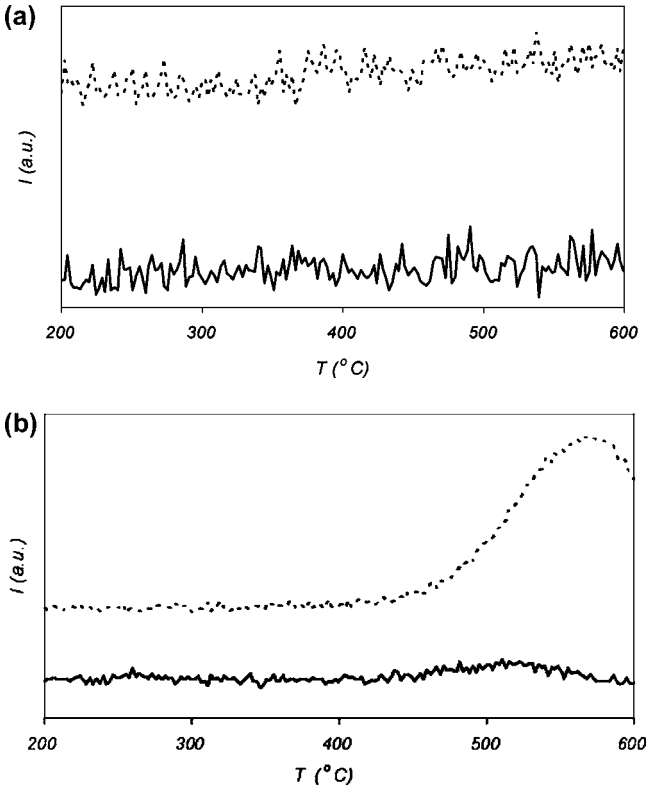

Figure 2. Emission of (a) NO and (b) NO_2 during the activity test after poisoning with piperidine for $LaMnO_3$ (solid line) and $La_{0.9}Sr_{0.1}MnO_3$ (dotted line).

such (Figure 2a). By contrast, for $LaMnO_3$, NO_2 poorly desorbed between 450 and 550 °C, whereas NO_2 release from the Sr-substituted catalyst was much more evident, always starting at ca. 450 °C (Figure 2b), possibly corresponding to NO accumulated over the surface and subsequently oxidized under the reaction atmosphere. Further NO_2 more weakly bound (i.e., in principle released below 450 °C) could not be detected because of the selected poisoning temperature.

From the present data, one may conclude that the N-containing molecule is completely oxidized at the selected temperature with the formation of NO_x species. Part of NO is immediately released from the samples (Figure 1), while part is retained, mostly in the presence of a higher concentration of oxygen vacancies, i.e., upon Sr addition, and it can be further oxidized to form NO_2. NO decomposition may also occur, leaving activated oxygen to saturate surface vacancies. The

dx.doi.org/10.1021/ic3015892 | Inorg. Chem. 2012, 51, 11680−11687

presence of methane in the reaction environment regenerates the active sites, inducing at least a negligible variation of activity if not even an increase of methane conversion due to the increased availability of activated oxygen species. Some literature data could support such hypotheses. Indeed, a competitive reoxidation process of the prereduced $LaCoO_3$ between NO and O_2 was revealed during reaction with CH_4. Under lean conditions (3 vol % O_2), negligible conversion of NO was detected until 500 °C even if above 450 °C CH_4 started to convert.[31]

However, in order to better support such an interpretation, some additional specific tests have been designed and described in the following.

3.2. Catalyst Characterization. The specific surface area of the as-prepared fresh catalysts was 70 $m^2\ g^{-1}$ for $LaMnO_3$ and 66 $m^2\ g^{-1}$ for $La_{0.9}Sr_{0.1}MnO_3$.

All of the present catalysts were characterized by high-phase purity because no reflection of extraneous phases has been observed in the XRD pattern even in the case of the Sr-doped sample. The main phase was rhombohedral $LaMnO_{3+\delta}$ (characterized by a double reflection at $2\theta \approx 33°$; JCPDS file 86-1234[18]). A detailed structural analysis has been reported elsewhere.[32] Some peak broadening has been observed because of the nanostructuring of the catalysts. No significant variation of the XRD pattern was observed for both the spent catalysts with respect to the fresh ones, except for a slight sharpening of the peak profile, corresponding to some particle sintering (Figure 3).

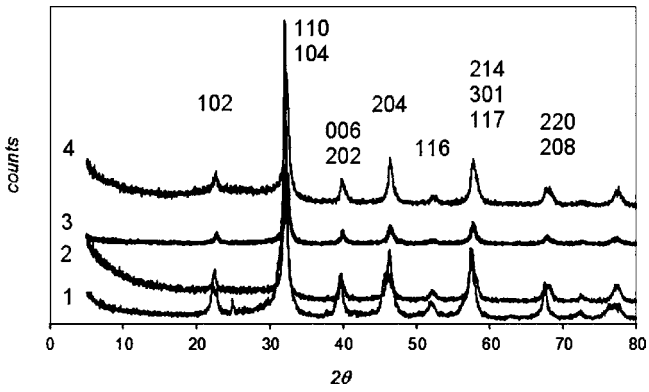

Figure 3. XRD patterns of (1) fresh $LaMnO_3$, (2) $LaMnO_3$ after 240 h of flow in pyridine, (3) fresh $La_{0.9}Sr_{0.1}MnO_3$, and (4) $La_{0.9}Sr_{0.1}MnO_3$ after 240 h of flow in pyridine.

Scanning electron microscopy analysis, already reported elsewhere,[6] confirmed the nanometric size (20−60 nm) of the samples analyzed here.

3.2.1. TPR and TGA. TPR was carried out after saturation in a O_2 flow. Two main reduction peaks may be noticed, occurring at 200−400 and 650−850 °C, respectively. The former evidenced a low-temperature shoulder, whose intensity increased upon doping with Sr (Figure 4). Such a shoulder was attributed to the reduction of Mn^{4+} to Mn^{3+}.[33] It should be noticed that some Mn^{4+} was present also in the oxidized undoped sample, but, of course, it increased with Sr addition. This confirms the presence of a higher amount of oxygen vacancies in the unpoisoned Sr-doped samples with respect to the undoped one.[33]

TGA was also carried out on the oxidized samples either in air flow or under inert gas. According to what was already

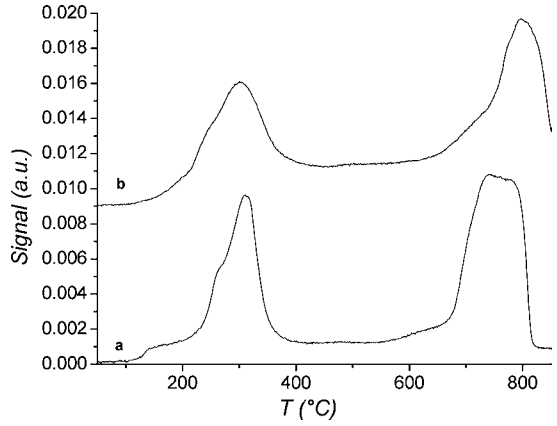

Figure 4. TPR profiles of samples $LaMnO_3$ (a) and $La_{0.9}Sr_{0.1}MnO_3$ (b).

reported for TPD of preadsorbed oxygen,[33] LaA′MnO_3 samples are characterized by high-temperature oxygen release starting at ca. 500 °C and by a low-temperature peak (denoted α), relevant in the case of Sr doping only, and usually ascribed to the release of surface oxygen.

From Figure 5, the weight loss of sample $La_{0.9}Sr_{0.1}MnO_3$ appears to be much higher than that of the undoped perovskite,

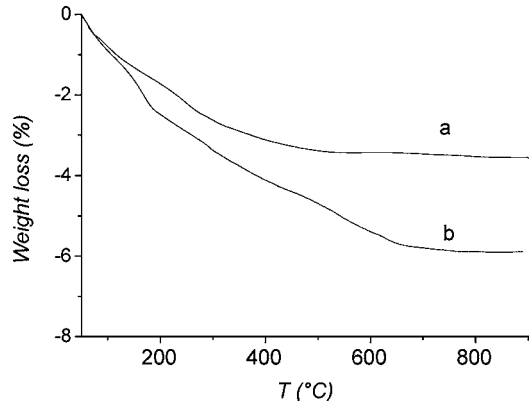

Figure 5. TGA patterns of samples $LaMnO_3$ (a) and $La_{0.9}Sr_{0.1}MnO_3$ (b).

confirming a higher availability of surface oxygen thanks to a higher amount of surface oxygen vacancies.

3.2.2. NO Adsorption/NO-TPD. NO adsorption at rt was carried out on the oxidized sample. The presence of Sr caused a relevant increment of NO adsorption. Indeed, the amount of NO adsorbed at rt was 15 and 19 μmol mg_{cat}^{-1} for the undoped and Sr-doped materials, respectively; i.e., ca. 20% increase was observed upon Sr addition.

The ability of perovskite-like materials for NO_x storage was already reported for $BaFeO_3$.[34] Furthermore, NO_x storage and reduction materials were described, in which Ba, Sr, and Ca are the A-site cations and Sn, Zr, and Ti the B-site ones.[35,36]

TPD tests after NO adsorption at rt revealed small qualitative differences between the two samples (Figure 6). No evolution of N_2O or N_2 was ever detected, whereas NO desorption started at 50 °C and it was not complete even at 500 °C, especially for the Sr-doped material. This is consistent with our activity data because peaks of NO were detected (Figure 1a) desorbing at 450 °C, with a higher retention by the Sr-doped material. Two main peaks can be recognized in Figure 6: the

dx.doi.org/10.1021/ic3015892 | Inorg. Chem. 2012, 51, 11680−11687

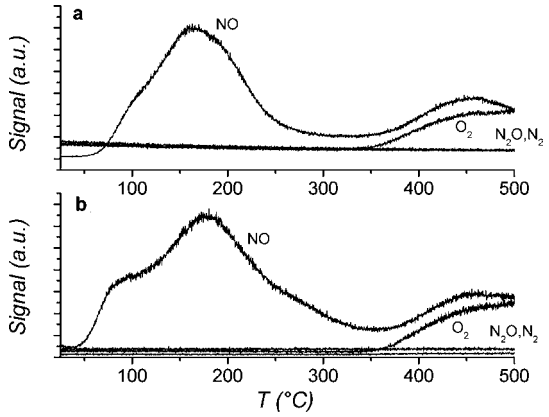

Figure 6. NO-TPD experiments for $LaMnO_3$ (a) and $La_{0.9}Sr_{0.1}MnO_3$ (b).

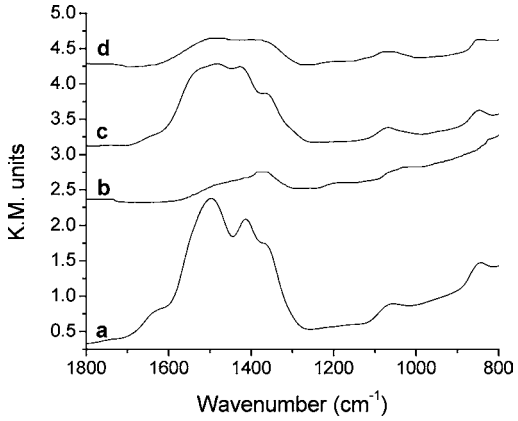

Figure 7. DRIFT spectra of $LaMnO_3$ before (a) and after (b) and $La_{0.9}Sr_{0.1}MnO_3$ before (c) and after (d) O_2 pretreatmet at 500 °C.

former, broad, with a shoulder at low temperature (50−110 °C) and a main component at 100−250 °C. A high-temperature peak was also detected above 350 °C and such are the species likely interesting in the present investigation, being stable and adsorbed at the selected reaction temperature for poisoning. The high-temperature desorption was also accompanied by O_2 evolution.

A similar situation was evidenced by Zhang et al.[37] for NO-TPD experiments on $La(Co, Mn)_{1-x}Cu_xO_3$, even if the high-temperature peak was shifted toward lower temperature, and the authors related the peaks to physisorbed NO, nitrosyl, and nitrate species, respectively. Moreover, the simultaneous desorption of O_2 at high temperature was suggested as further evidence of nitrate decomposition during desorption. Our data partially contradict such a attribution because IR analysis (vide infra) evidenced adsorbed nitrates and nitrosyls but not physisorbed NO. It was also reported that adsorbed nitrates can decompose above 300 °C into NO and O_2.[38−42]

3.2.3. DRIFT Analysis. The infrared (IR) spectra of NO adsorbed on $LaMnO_3$ showed bands of dinitrosyl, nitrite, and nitrate species. Therefore, NO interacts both through Mn^{3+} ions (dynitrosyls) or through O^{2-} ions (nitrites and nitrates). Whatever is the adsorption process, blocking of the active sites responsible for methane oxidation in the low-temperature range via the suprafacial mechanism occurs. In principle, thus, a decrease of the activity should be expected.

In order to evaluate the surface properties of the materials, the samples were monitored by means of DRIFT spectroscopy after NO saturation. In Figure 7, the spectra of the samples before and after treatment in O_2 (20 vol %) at 500 °C are reported. Before treatment in O_2, the surface of the materials was principally covered by adsorbed carbonates, even if a small broad band above 1600 cm^{-1} evidenced the presence of a minor quantity of hydrogen carbonates,[43] produced by the adsorption of atmospheric CO_2, as evidenced by the broad IR adsorption in the region 1700−1300 cm^{-1} due to the convolution of components at 1630, 1540, 1490, 1420, and 1360 cm^{-1}. Moreover, two small bands are present at 1065 and 850 cm^{-1}. Sr doping did not relevantly influence the nature of the carbonate species adsorbed on the surface, and the detected bands may be mainly related to the presence of mono- and bidentate carbonates. Hodjati et al.[36] assigned the bands at 850, 1060, and 1430 cm^{-1} to monodentate carbonate. Adsorption of CO and CO_2 on cerium oxide led to both monodentate (1454, 1348, 1062, and 854 cm^{-1}) and bidentate (1562, 1286, 1028, and 854 cm^{-1}) carbonates.[44] Other authors reported the formation of monodentate carbonates over amorphous aluminum oxide when it was in contact with a solution of either Na_2CO_3 or $NaHCO_3$, which were evidenced by two bands at 1420 and 1484 cm^{-1}.[43] After treatment in O_2 at 500 °C, the intensity of the bands significantly decreased, even if a broad adsorption between 1600 and 1300 cm^{-1} and small bands at 850 and 1060 cm^{-1} were still detectable. The broad signal principally derives from a band at 1360 cm^{-1} and one at 1490 cm^{-1}, and therefore we may conclude that under such pretreatment conditions the elimination of surface carbonates was not complete.

After exposure to NO (1 vol % in He) at rt, new bands appeared in the region 1300−1600 cm^{-1} (Figure 8). Four

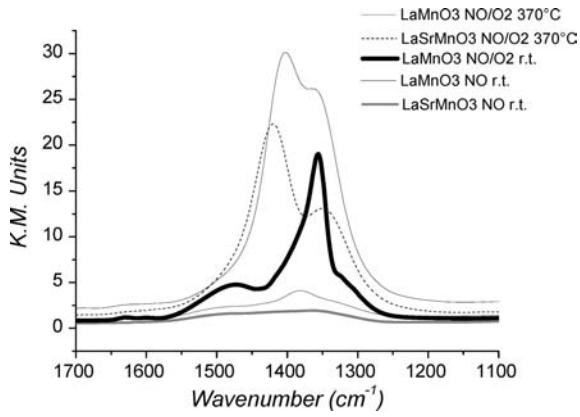

Figure 8. DRIFT spectra of NO-saturated samples: $LaMnO_3$ at rt under 1% NO, at 370 °C under a NO/O_2 mixture, and at rt with a NO/O_2 mixture; $La_{0.9}Sr_{0.1}MnO_3$ at rt under 1% NO and at 370 °C under a NO/O_2 mixture.

bands at 1320, 1370, 1410, and 1480 cm^{-1} became evident for $LaMnO_3$, while for $La_{0.9}Sr_{0.1}MnO_3$, the main components were at 1320, 1360, 1420, and 1480 cm^{-1}. Treatment in diluted NO at higher temperature (370 °C) did not cause any significant change in the IR patterns (not shown), but as soon as oxygen was fed together with NO, a strong increase in the adsorption intensity and a change in the IR adsorption profile occurred (Figure 8). Two intense bands at 1410 and 1350 cm^{-1} and at 1420 and 1350 cm^{-1} appeared for the undoped and Sr-doped samples, respectively. As was already reminded, NO can generate dinitrosyl species interacting with Mn^{3+} ions or

dx.doi.org/10.1021/ic3015892 | Inorg. Chem. 2012, 51, 11680−11687

nitrites and nitrates with O^{2-} when it adsorbs on $LaMnO_3$.[29] The absence of bands above 1600 cm^{-1} has already been attributed to the lack of dinitrosyl upon interaction between NO and metallic ions.[45] So, the adsorption of NO mainly led to the formation of adsorbed nitrate/nitrite species because of the redox properties of these materials. The IR identification of these species is controversial because their characteristic IR bands appear in the same region, 1600−1000 cm^{-1}. Before adsorption, NO can be oxidized to NO_2, which can form surface nitrite or be further oxidized to nitrates upon interaction with activated oxygen.[46] Peña et al. revealed the formation of monodentate and bidentate nitrates interacting with the transition-metal cations on $LaMnO_3$ after exposure to NO, correlated to the bands appearing at 1610, 1485, 1135, and 1045 cm^{-1}.[47] Two bands at 1341 and 1436 cm^{-1} after treatment in NO/O_2 at 400 °C of $BaFeO_3$ were attributed to monodentate nitrates over barium while bands at 1360 and 1417 cm^{-1} were generically attributed to nitrates on perovskite.[48] An NO, NO_2, and O_2 mixture caused the appearance of bands at 1360, 1385, and 1470 cm^{-1} on $BaSnO_3$. The authors associated the band at 1385 cm^{-1} with free nitrates and the couple of bands at 1360 and 1470 cm^{-1} with N-bound nitrate species.[36]

To further evaluate the nature of the adsorbed species and their evolution with temperature, we exposed the NO-saturated $LaMnO_3$ sample to a NO/O_2 mixture at rt (Figure 8). The intensity of the bands significantly increased with respect to the same experiment carried out at 370 °C, without the formation of new ones. Indeed, the effect was more evident for the band at 1370 cm^{-1}, which also blue-shifted to 1360 cm^{-1}, while the intensity ratio was constant for the other bands and their position was almost unchanged. We ascribed it to the formation of nitrate species of different nature on our samples already by oxidation of NO ar rt. In particular, the band around 1370 cm^{-1} was previously assigned to the formation of free ionic nitrates on Ba,[49,50] while generally for inorganic nitrate salts, a band appeared around 1380 cm^{-1}.[51] The attribution of the other bands is more complex because of their broad overlap, but we can generally assign them to mono- and bidentate nitrates. Tentatively, we can suppose that the couple of bands at 1320 and 1410 cm^{-1} belong to monodentate nitrates, while the band at 1490 cm^{-1} may be related to bidentate nitrates, with the symmetric stretching of NO_2 around 1300 cm^{-1} hidden by the broad absorption. A couple of bands at 1337 and 1436 cm^{-1} was already revealed by Abdulhamid et al. for monodentate nitrates over Ba.[52] Moreover, the splitting between the symmetric and antisymmetric stretching ν_3 vibrational modes, which arises upon coordination of nitrates, can be considered an index to identify the nature of the surface species.[51,53,54] A relatively small splitting is typical for monodentate nitrates, while a big one is shown by bidentate ones. When NO/O_2 was fed at high temperature, mainly monodentate nitrates developed. The slight blue shift of the symmetric stretching vibration for the undoped sample could be due to overlap with masked free nitrate bands.

The presence of O_2 in the feed favors the storage of NO as nitrate, mainly in a free ionic form but also more interacting ones (mono- and bidentate) on $LaMnO_3$ at rt. At higher temperature, the amount of NO adsorbed significantly increased and the nature of the species changed. In particular, the relative amounts of monodentate nitrates (1420 and 1320 cm^{-1}) became predominant. The presence of Sr seems to influence the formation of nitrates. A higher amount of more interacting nitrate species (mono- and bidentate) was formed in comparison to free ionic ones when Sr was present.

Finally, the samples were analyzed in a mixture of NO + O_2 at 370 °C. A band at 1370 cm^{-1} increased its intensity with the Sr-doped sample, progressively shifting at 1384 cm^{-1}, typical of ionic nitrates. Keeping the sample under the same flow, after ca. 30 min on-stream this band split into two bands, keeping their intensity ratio unaltered while increasing their intensity, and were assigned to monodentate nitrates. Similar behavior characterized the undoped sample, although with a much lower intensity.

CH_4 was dosed after saturation at 370 °C with NO, CH_4/O_2, and $CH_4/O_2/NO$ in different proportions, but no differences in the spectra were observed.

This would indicate that NO evolves to nitrites and nitrates under an oxidizing atmosphere, but such species do not interact directly with methane as long as they are stable on the catalyst surface. Therefore, a two-step mechanism is confirmed for the interaction of methane with activated oxygen, formed upon decomposition of adsorbed NO.

4. CONCLUSIONS

The effect of N-containing model molecules, mimicking possible poisons occurring in BG streams, has been investigated during the catalytic combustion of methane. Sr-doped and undoped manganites were evaluated. Such catalysts were found to be particularly active and resistant to sulfur poisoning.

A different behavior was observed for the two catalysts: the undoped sample decreased its activity upon injection of the N-based impurities, while for the doped one, an increase of methane conversion after injection was observed.

A possible mechanism was proposed, starting with combustion of the N-containing molecule to form NO. The latter may be released from the catalyst or remain partly adsorbed over oxygen vacancies, more likely in the case of the Sr-containing sample, as confirmed by TPR and NO adsorption experiments. NO evolved under an oxidizing atmosphere to nitrate or decomposed, leaving activated oxygen on the surface. The latter is involved in the additional conversion of methane observed for the "poisoned" $La_{0.9}Sr_{0.1}MnO_3$.

AUTHOR INFORMATION

Corresponding Author

*E-mail: ilenia.rossetti@unimi.it.

Present Address

[§]Department of Chemical Engineering, University of California, Santa Barbara, CA 93106.

Notes

The authors declare no competing financial interest.

REFERENCES

(1) Seiyama, T. In *Properties and applications of the Perovskite-type oxides*; Tejuca, G., Fierro, J. L. G., Eds.; Marcel Dekker: New York, 1993.
(2) Nakamura, T.; Misono, M.; Yoneda, Y. *J. Catal.* **1983**, *83*, 151.
(3) Ponce, S.; Peña, M. A.; Fierro, J. L. G. *Appl. Catal., B* **2000**, *24*, 193.
(4) Ferri, D.; Forni, L. *Appl. Catal., B* **1998**, *16*, 119.
(5) Wold, A.; Arnott, R. J. *J. Phys. Chem. Solids* **1959**, *9*, 176.
(6) Rossetti, I.; Buchneva, O.; Biffi, C.; Rizza, R. *Appl. Catal., B* **2009**, *89*, 383.
(7) Li, W. In *Properties and applications of the Perovskite-type oxides*; Tejuca, G., Fierro, J. L. G., Eds.; Marcel Dekker: New York, 1993.

(8) Tejuca, L. G.; Fierro, J. L. G.; Tascón, J. M. D. *Adv. Catal.* **1989**, *36*, 237.
(9) Rosso, I.; Saracco, G.; Specchia, V.; Garrone, E. *Appl. Catal., B* **2003**, *40*, 195.
(10) Buchneva, O.; Rossetti, I.; Biffi, C.; Allieta, M.; Kryukov, A.; Lebedeva, N. *Appl. Catal., A* **2009**, *370*, 24.
(11) Buchneva, O.; Rossetti, I.; Oliva, C.; Scavini, M.; Capelli, S.; Sironi, B.; Allieta, M.; Kruykov, A.; Forni, L. *J. Mater. Chem.* **2010**, *20*, 10021.
(12) Guo, X.; Tak, J. K.; Johnson, R. L. *J. Hazard. Mater.* **2009**, *166*, 372.
(13) Rasi, S.; Veijanen, A.; Rintala, J. *Energy* **2007**, *32*, 1375.
(14) Escandon, L. S.; Hevia, M. A. G.; Paredes, J. R.; Hurtado, P.; Ordonez, S.; Diez, F. V. NATO/CCMS Pilot Study. EPA Report 625CR-02/003, 2002; p 22.
(15) Ramel, M. *Stud. Environ. Sci.* **1994**, *61*, 145.
(16) Smet, E.; Van Langenhove, H.; De Boo, I. *Atmos. Environ.* **1999**, *33*, 1295.
(17) Chiarello, G. L.; Rossetti, I.; Forni, L. *J. Catal.* **2005**, *236*, 251.
(18) *Selected Powder Diffraction Data for Minerals*; DBM 1−40; JCPDS: Swarthmore, PA, 1974−1992.
(19) Dal Santo, V.; Dossi, C.; Fusi, A.; Psaro, R.; Mondelli, C.; Recchia, S. *Talanta* **2005**, *66*, 674.
(20) Voorhoeve, R. J. H.; Remeika, J. P.; Johnson, D. W. *Science* **1973**, *180*, 62.
(21) Auer, R.; Alifanti, M.; Delmon, B.; Thyrion, F. *Appl. Catal., B* **2002**, *39*, 311.
(22) Hurtado, P.; Ordonez, S.; Vega, A.; Diez, F. *Chemosphere* **2004**, *55*, 681.
(23) Hurtado, P.; Ordonez, S.; Sastre, H.; Diez, F. *Appl. Catal., B* **2004**, *47*, 85.
(24) Koger, S.; Bockhorn, H. *Proc. Combustion Inst.* **2005**, *30*, 1201.
(25) Ninomiya, Y.; Dong, Z.; Suzuki, Y.; Koketsu, J. *Fuel* **2000**, *79*, 449.
(26) Mackie, J. C.; Colket, M. B.; Nelson, P. F.; Elser, M. *Int. J. Chem. Kinet.* **1991**, *23*, 733.
(27) Zhang, X.; Walters, A. B.; Vannice, M. A. *J. Catal.* **1995**, *155*, 290.
(28) Busca, G.; Lietti, L.; Ramis, G. M.; Berti, F. *Appl. Catal., B* **1998**, *18*, 1.
(29) Peña, M. A.; Fierro, J. L. G. *Chem. Rev.* **2001**, *101*, 1981.
(30) Shi, C.; Walters, A. B.; Vannice, M. A. *Appl. Catal., B* **1997**, *14*, 175.
(31) Pirez-Engelmann, M.; Granger, P.; Leclercq, L.; Leclercq, G. *Top. Catal.* **2004**, *30/31*, 59.
(32) Oliva, C.; Allieta, M.; Scavini, M.; Biffi, C.; Rossetti, I.; Forni, L. *Inorg. Chem.* **2012**.
(33) Rossetti, I.; Biffi, C.; Forni, L. *Chem. Eng. J.* **2010**, *162*, 768.
(34) Xian, H.; Zhang, X.; Li, X.; Zou, H.; Meng, M.; Li, Q.; Tan, Y.; Tsubaki, N. *J. Phys. Chem.* **2010**, *114*, 11844.
(35) Hodjati, S.; Vaezzadeh, K.; Petit, C.; Pitchon, V.; Kiennemann, A. *Appl. Catal., B* **2000**, *26*, 5.
(36) Hodjati, S.; Petit, C.; Pitchon, V.; Kiennemann, A. *Appl. Catal., B* **2000**, *27*, 117.
(37) Zhang, R.; Villanueva, A.; Alamdari, H.; Kaliaguine, S. *J. Mol. Catal. A: Chem.* **2006**, *258*, 22.
(38) Zhang, R. D.; Villanueva, A.; Alamdari, H.; Kaliaguine, S. *Appl. Catal., B* **2006**, *64*, 220.
(39) Zhang, R. D.; Villanueva, A.; Alamdari, H.; Kaliaguine, S. *Appl. Catal., A* **2006**, *263*, 85.
(40) Zhang, R. D.; Villanueva, A.; Alamdari, H.; Kaliaguine, S. *J. Catal.* **2006**, *237*, 368.
(41) She, X.; Flytzani-Stephanopoulos, M. *J. Catal.* **2006**, *237*, 79.
(42) Coq, B.; Tachon, D.; Figueras, F.; Mabilon, G.; Prigent, M. *Appl. Catal., B* **1995**, *6*, 271.
(43) Su, C.; Suarez, D. L. *Clays Clay Miner.* **1997**, *45*, 814.
(44) Li, C.; Sakata, Y.; Arai, T.; Domen, K.; Maruya, K.-i.; Onishi, T. *J. Chem. Soc., Faraday Trans.* **1989**, *1* (85), 929.
(45) Forni, L.; Oliva, C.; Barzetti, T.; Selli, E.; Ezerets, A. M.; Vishniakov, A. V. *Appl. Catal., B* **1997**, *13*, 35.
(46) Isupova, L. A.; Budneva, A. A.; Paukshtis, E. A.; Sadykov, V. A. *J. Mol. Catal. A: Chem.* **2000**, *158*, 275.
(47) Peña, M. A.; Tascon, J. M. D.; Fierro, J. L. G.; Gonzalez Tejuca, L. *J. Colloid Interface Sci.* **1987**, *119*, 100.
(48) Xian, X.; Zhang, X.; Li, X.; Li, L.; Zou, H.; Meng, M.; Li, Q.; Tan, Y.; Tsubaki, N. *J. Phys. Chem. C* **2010**, *114*, 11844.
(49) Sedlmair, Ch.; Seshan, K.; Jentys, A.; Lercher, J. A. *J. Catal.* **2003**, *214*, 308.
(50) Westerberg, B.; Fridell, E. *J. Mol. Catal. A: Chem.* **2001**, *165*, 249.
(51) Davydov, A. A. *Infrared Spectroscopy of Adsorbed Species on the Surface of Transition Metal Oxides*; Wiley: New York, 1990.
(52) Abdulhamid, H.; Dawody, J.; Fridell, E.; Skoglundh, M. *J. Catal.* **2006**, *244*, 169.
(53) Westerberg, B.; Fridell, E. *J. Mol. Catal. A: Chem.* **2001**, *165*, 249.
(54) Fanson, P. T.; Horton, M. R.; Delgass, W. N.; Lauterbach, J. *Appl. Catal., B* **2003**, *46*, 393.